Primer Extension Assay

Ten micrograms of total RNA with 0.5 pmol oligodeoxynucleotide primer that was conjugated with either AlexaFluor®488 or fluorescein (FAM) was heat denatured for 1 min at 95°C. Following a 10 min hybridization step at 43°C, reverse transcription was carried out in a buffer containing 200 units of M-MLV reverse transcriptase (Promega, USA) in the presence of either 1 mM dNTP or 0.004 mM dNTP. For the sequencing reactions, dideoxynucleotides were added to a final concentration of 0.06 mM. cDNA products were ethanol precipitated and primer extension products were resolved on a denaturing gel (6% polyacrylamide and 8 M urea) and visualized by scanning using a Typhoon Analyzer (Amersham). For sequencing ladders, a control rRNA gene sequence was obtained by PCR amplification of C57BL/6J genomic DNA with specific primers for the U50-sites (from 2537 bp to 2662 bp of the 28S rRNA gene), and the PCR product was cloned into a TA vector (Promega, USA). The primers that were used are listed in Table S2.

Real-time qPCR

RNA samples were treated with DNase I (Invitrogen), and then converted to cDNA using an oligo-dT primer and the SuperScript® First-strand synthesis system for RT-PCR (Invitrogen). qPCR was carried out using TaqMan® gene expression assay (ABI Inc., USA) and SYBR Green I® PCR Master Mix (ABI) with a Prism 7000 Real-time PCR System (ABI). Three technical replicates were run per sample. For the SYBR-based qPCR analysis, we tried several sets of PCR primers for each gene. The efficiency of each primer set was tested with serial dilutions of cDNA, and the combination of primers that yielded the best single amplified product was selected by checking for a single sharp peak in the dissociation curve of each product. The cycle threshold value (Ct) of each target gene was normalized relative to the reference genes (see below). All primer sets, except those for the TaqMan® assays, were designed using Primer3 via the NCBI webpage (http://www.ncbi.nlm.nih.gov/tools/primer-blast/) and are listed in Table S2.

To select appropriate reference genes for the survey of gene expression in various organs, we used the RefGenes tool from the Genevestigator platform [44] and selected the three top-ranking genes, *Tbc1d25*, *Bud13*, and *Krt81* (Fig. S5A). Microarray analysis confirmed that these genes were expressed equally in wild-type and $\Delta mU50_{(HG\text{-}b)}$ mice and that their signal intensities were at adequate levels but not as high as the signal intensity of the housekeeping *Actb* gene (Fig. S5B). We failed to obtain optimal amplification conditions for *Krt81*, but qPCR analyses showed that both *Tbc1d25* and *Bud13* yielded comparable expression levels (a reciprocal number of Ct value) among the eight organs analyzed (Fig. S5C). Based on these findings, we used *Tbc1d25* as a reference in all the qPCR analyses in this study.

PCR-SSCP

The cDNA library was constructed using a miScript system (QIAGEN, Germany) according to the manufacturer's instruction. Control plasmids containing individual mU50 variants were cloned into a pGEM-T easy vector (Promega). PCR primers for the mU50 sequence (forward, 5′-TCTATGATGATCCTATCCCG-3′; reverse, 5′-ATCTCAGAAGCCAGATCCGT-3′) were labeled with either AlexaFluor®647 or 6-carboxyfluorescein (6-FAM) at the 5′-ends. In the PCR reaction, 2 ng of template cDNA was used and amplified for 30 cycles. The PCR product was diluted to 1:125 with a loading buffer (96% deionized formamide containing 10 mM EDTA, 0.01% bromophenol blue), denatured at 95°C for 10 min, and applied to an acrylamide sequencing gel (10% native PAGE (aa:bis = 19:1) in 1×TBE). The gels were run at 1000 V (25V/cm) for 190 min at 22°C and scanned using a Typhoon scanner (GE Biosciences).

DNA Microarray

Microarray analysis was performed at the core facility of Cell Innovator Inc. (Fukuoka, Japan). Total RNA from splenic B-cells (23 weeks old; three samples per genotype) was purified with RNeasy Micro kit (QIAGEN). The quality of the RNA was assessed by monitoring the absorbance at 260 and 280 nm and rRNA fragmentation was measured using a Bioanalyzer (Agilent Technologies, USA). Concentrations of purified RNA samples were determined using a Nanodrop spectrophotometer (ND-1000; Thermo Scientific, USA) and equal amounts of the three RNA samples were mixed. cRNA was hybridized to a GeneChip® Microarray (Mouse Expression 430 2.0 Array, Affymetrix, USA) containing 45,101 probes that cover more than 20,000 mouse genes. The expression value and detection calls were computed from the raw data following the procedures outlined for the Affymetrix Microarray Suite software version 5.0. A complete gene list of the microarray analyses was built using GeneSpring software version 7.3.1 (Silicon Genetics Inc., USA). Because arranged immunoglobulin (Ig) genes could not be distinguished in the mixed samples, we omitted the probes for Ig genes from the analysis.

Data Deposition

The microarray data have been deposited and are available online in the Gene Expression Omnibus (GEO) database (http://www.ncbi.nlm.nih.gov/geo/) under the accession number GSE41164.

Supporting Information

Figure S1 Structural bases of mU50 snoRNA. (A) Computer-assisted prediction of the secondary structure of mU50 snoRNA variants. The k-turn structure that might possibly be formed by box C and D motifs was not taken into account for the prediction. Note that the all three variants exhibit the identical structure at the most stable energy states. (B) Sequence similarity among human and mouse U50 snoRNAs. Human U50A and U50B snoRNAs (formerly U50 and U50' in [17]) are compared with the mU50 snoRNA sequence. Conserved box motifs are indicated by rectangles. Antisense elements to 28S rRNA are indicated by broken lines. The four U residues in the U50A snoRNA (shown in red and underscored) are where a genomic TT-deletion has been reported in prostate and breast cancers [18,19]. (C) Schematic representation and nucleotide sequences of the mU50 snoRNA target sites (in orange) on the rRNA gene in five organisms. The segments down-stream of the mU50-sites (gray rectangles) are variable having expanded in size through insertions and/or duplications during the evolutionary process. A further comparative genomic data analysis indicated that the U50-sites are highly conserved from archaea to vertebrate. Referring to a previous report of the *T. thermophilus* 23S rRNA structure [32], the conserved site for the mU50-sites is subject to form the loop 62 which participates in the formation of the inter-subunit bridge. (PDF)

Figure S2 Nucleotide sequences of the modified *mU50HG-b* gene in comparison with the original sequence in wild-type. The sequence starts from the intron 3 which contains an mU50 snoRNA sequence (upstream) through the intron 4 where another mU50 sequence (downstream) resides. mU50 snoRNA and exon sequences are shown in blue and black

background, respectively. Nucleotides unaltered upon the recombination are connected with asterisks. The upstream mU50 sequence is completely replaced with a non-coding sequence derived from pBluescript II plasmid, and the downstream mU50 sequence is replaced with residual nucleotides of the loxP-*Neo*^{r}-loxP cassette after the Cre-lox recombination. Note that the sizes of the modified introns are identical to those of wild-type.
(PDF)

Figure S3 Phenotypes of the mU50-deficient animals. (A) Weight gain of female and male ΔmU50$_{(HG\text{-}b)}$ and wild-type mice (n = 14 per genotype). A plot of ΔmU50$_{(HG\text{-}b)}$ mice was always lower than that of the wild-type mice throughout the observation period, although this difference was not statistically significant. Error bars = 1. S.D. (standard deviation) (B) Average tissue weight (% body-weight) in wild-type and ΔmU50$_{(HG\text{-}b)}$ mutant mice at 10 weeks after birth (n = 7 per genotype). Although some organs such as heart, liver, and testis of ΔmU50$_{(HG\text{-}b)}$ mice were lighter than the same organs in wild-type, no prominent differences were found in their morphology and histology (data not shown). Error bars = 1 S.D. *P<0.05. (C) Age-associated changes in the number of peripheral lymphocytes (n = 4 per genotype) in ΔmU50$_{(HG\text{-}b)}$ and wild-type mice. Fitted curves for ΔmU50$_{(HG\text{-}b)}$ (broken line) and wild-type (solid line) are indicated. (D) Proliferation activity of splenocytes *in vitro*. For cell culture, 2×10^5 of isolated splenocytes from individual genotypes were grown on 6-well plates (BD Falcon, USA) in the presence of 1.0 μg/ml of lipopolysaccharides (Sigma, USA) as a stimulus. The numbers of cells were counted with a hemocytometer. The number of cells 24 h after inoculation was designated as 100%. Error bars = 1 S.D. from three independent assays.
(PDF)

Figure S4 Representative data of qPCR validation of relative gene expression in splenocytes between wild-type and ΔmU50$_{(HG\text{-}b)}$ mice. The threshold value was normalized by the beta-actin gene (*Actb*) according to the $\Delta\Delta$Ct method. Error bars = 1 S.D. for three biological replicates. *P<0.05; WT: wild-type; Δ: ΔmU50$_{(HG\text{-}b)}$ mice.
(PDF)

Figure S5 Selection of qPCR reference genes for assessment of organ-dependent gene expression patterns. (A) A result view of RefGenes platform [44] on inquiry for appropriate reference genes for qPCR survey to eight organs. The 3 top-ranking candidates were *Tbc1d25*, *Bud13*, and *Kit81*. (B) Comparable expression levels of the candidate genes obtained from microarray analysis of splenic B-cells in wild-type and ΔmU50$_{(HG\text{-}b)}$ mice. (C) TaqMan®-based qPCR analyses of the candidate genes in various organs of wild-type mice. The expression levels (a reciprocal number of Ct value) of reference genes among eight organs are compared. Note that both *Tbc1d25* and *Bud13* showed less inter-organ variations in their expression levels as compared to those of *Actb*.
(PDF)

Figure S6 Comparative genomic analyses of human and mouse mU50 host-gene promoter sites. (A) The phylogenetic tree was constructed based on the promoter sequences (from −2,000 bp behind 5′TOP transcription start site to +500 bp) of these U50 snoRNA host-genes using VISTA tools for comparative genomics that is provided by Lawrence Berkeley National Laboratory (http://genome.lbl.gov/vista/index.shtml). The results support the closest promoter sequence of *mU50HG-b* to human *U50HG*. (B) Conservation of promoter sequences among human and mouse U50 host-genes. Highly conserved loci (>70% similarity) with human *U50HG* are shown in pink.
(PDF)

Table S1 Anomalies detected in age-matched wild-type and ΔmU50$_{(HG\text{-}b)}$ mice. Age-matched mice that were euthanized or had died were examined pathologically (n = 40 per genotype).
(DOC)

Table S2 List of PCR primers used in this study.
(DOC)

Acknowledgments

We thank to Drs. Hitoshi Satoh and Tetsuro Hirose for valuable discussion on the generation of the mouse model.

Author Contributions

Conceived and designed the experiments: Y. Soeno MA S. Kakuta RTF SM TA. Performed the experiments: Y. Soeno KF TK YT Y. Shimazu KS S. Kubo. Analyzed the data: Y. Soeno MA S. Kakuta KS TA. Contributed reagents/materials/analysis tools: S. Kubo YI YN SM. Wrote the paper: Y. Soeno TA.

References

1. Matera AG, Terns RM, Terns MP (2007) Non-coding RNAs: lessons from the small nuclear and small nucleolar RNAs. Nat Rev Mol Cell Biol 8: 209–220.
2. Williams GT, Farzaneh F (2012) Are snoRNAs and snoRNA host genes new players in cancer? Nat Rev Cancer 12: 84–88.
3. Kiss-Laszlo Z, Henry Y, Bachellerie JP (1996) Site-specific ribose methylation of preribosomal RNA: a novel function for small nucleolar RNAs. Cell 85: 1077–1088.
4. Kiss-Laszlo Z, Henry Y, Kiss T (1998) Sequence and structural elements of methylation guide snoRNAs essential for site-specific ribose methylation of pre-rRNA. EMBO J 17: 797–807.
5. Bachellerie JP, Cavaillé J, Hüttenhofer A (2002) The expanding snoRNA world. Biochimie 84: 775–790.
6. Hüttenhofer A, Brosius J, Bachellerie JP (2002) RNomics: identification and function of small, non-messenger RNAs. Curr Opin Chem Biol 6: 835–843.
7. Filipowicz W, Pogacic V (2002) Biogenesis of small nucleolar ribonucleoproteins. Curr Opin Cell Biol 14: 319–327.
8. Kiss T (2002) Small nucleolar RNAs: an abundant group of noncoding RNAs with diverse cellular functions. Cell 109: 145–148.
9. Dieci G, Preti M, Montanini B (2009) Eukaryotic snoRNAs: A paradigm for gene expression flexibility. Genomics 94: 83–88.
10. Richard P, Kiss AM, Darzacq X, Kiss T (2006) Cotranscriptional recognition of human intronic box H/ACA snoRNAs occurs in a splicing-independent manner. Mol Cell Biol 26: 2540–2549.
11. Tycowski KT, Shu MD, Steitz JA (1996) A mammalian gene with introns instead of exons generating stable RNA products. Nature 379: 464–466.
12. Pelczar P, Filipowicz W (1998) The host gene for intronic U17 small nucleolar RNAs in mammals has no protein-coding potential and is a member of the 5′-terminal oligopyrimidine gene family. Mol Cell Biol 18: 4509–4518.
13. Smith CM, Steitz JA (1998) Classification of gas5 as a multi-small-nucleolar-RNA (snoRNA) host gene and a member of the 5′-terminal oligopyrimidine gene family reveals common features of snoRNA host genes. Mol Cell Biol 18: 6897–6909.
14. Lowe TM, Eddy SR (1999) A computational screen for methylation guide snoRNAs in yeast. Science 283: 1168–1171.
15. Esguerra J, Warringer J, Blomberg A (2008) Functional importance of individual rRNA 2′-O-ribose methylations revealed by high-resolution phenotyping. RNA 14: 649–656.
16. Esteller M (2011) Non-coding RNAs in human disease. Nat Rev Genet 12: 861–874.
17. Tanaka R, Satoh H, Moriyama M, Satoh K, Morishita Y, et al. (2000) Intronic U50 small-nucleolar-RNA (snoRNA) host gene of no protein-coding potential is mapped at the chromosome breakpoint t(3;6)(q27;q15) of human B-cell lymphoma. Genes Cells 5: 277–287.
18. Dong X-Y, Rodriguez C, Guo P, Sun X, Talbot JT, et al. (2008) SnoRNA U50 is a candidate tumor-suppressor gene at 6q14.3 with a mutation associated with clinically significant prostate cancer. Hum Mol Genet 17: 1031–1042.

19. Dong X-Y, Guo P, Boyd J, Sun X, Li Q, et al. (2009) Implication of snoRNA U50 in human breast cancer. J Genet Genomics 36: 447–454.
20. Tanaka-Fujita R, Soeno Y, Satoh H, Nakamura Y, Mori S (2007) Human and mouse protein-noncoding snoRNA host genes with dissimilar nucleotide sequences show chromosomal synteny. RNA 13: 811–816.
21. Sakai K, Miyazaki J (1997) A transgenic mouse line that retains Cre recombinase activity in mature oocytes irrespective of the cre transgene transmission. Biochem Biophys Res Commun 237: 318–324.
22. Fernandez PC, Frank SR, Wang L, Schroeder M, Liu S, et al. (2003) Genomic targets of the human c-Myc protein. Gene Dev 17: 1115–1129.
23. Skryabin BV, Gubar LV, Seeger B, Pfeiffer J, Handel S, et al. (2007) Deletion of the MBII-85 snoRNA gene cluster in mice results in postnatal growth retardation. PLoS Genet 3: e235.
24. Ding F, Li HH, Zhang S, Solomon NM, Camper SA, et al. (2008) SnoRNA Snord116 (Pwcr1/MBII-85) deletion causes growth deficiency and hyperphagia in mice. PLoS ONE 3: e1709.
25. Cohen DI, Steinberg AD, Paul WE, Davis MM (1985) Expression of an X-linked gene family (XLR) in late-stage B cells and its alteration by the xid mutation. Nature 314: 372–374.
26. Nakajima M, Miyamoto Y, Ikegawa S (2011) Cloning and characterization of the osteoarthritis-associated gene DVWA. J Bone Miner Metab 29: 300–308.
27. Vitali P, Basyuk E, Le Meur E, Bertrand E, Muscatelli F, et al. (2005) ADAR2-mediated editing of RNA substrates in the nucleolus is inhibited by C/D small nucleolar RNAs. J Cell Biol 169: 745–753.
28. Kishore S, Stamm S (2006) The snoRNA HBII-52 regulates alternative splicing of the serotonin receptor 2C. Science 311: 230–232.
29. Schoemaker RJW, Gultyaev AP (2006) Computer simulation of chaperone effects of archaeal C/D box sRNA binding on rRNA folding. Nucleic Acids Res 34: 2015–2026.
30. Vos MJ, Hageman J, Carra S, Kampinga HH (2008) Structural and functional diversities between members of the human HSPB, HSPH, HSPA, and DNAJ chaperone families. Biochemistry 47: 7001–7011.
31. Baxter-Roshek JL, Petrov AN, Dinman JD (2007) Optimization of ribosome structure and function by rRNA base modification. PLoS ONE 2: e174. doi:10.1371/journal.pone.0000174.
32. Yusupov MM, YusupovaGZ, Baucom A, Lieberman K, Earnest TN, et al. (2001) Crystal structure of the ribosome at 5.5 Å resolution. Science 292: 883–896.
33. Decatur WA, Fournier MJ (2002) rRNA modifications and ribosome function. Trends Biochem Sci 27: 344–351.
34. Brimacombe R, Mitchell P, Osswald M, Stade K, Bochkariov D (1993) Clustering of modified nucleotides at the functional center of bacterial ribosomal RNA. FASEB J 7: 161–167.
35. Maquat LE (2004) Nonsense-mediated mRNA decay: splicing, translation and mRNP dynamics. Nat Rev Mol Cell Biol 5: 89–99.
36. Makarova JA, Kramerov DA (2005) Noncoding RNA of U87 host gene is associated with ribosomes and is relatively resistant to nonsense-mediated decay. Gene 363: 51–60.
37. Ender C, Krek A, Friedländer MR, Beitzinger M, Weinmann L, et al. (2008) A human snoRNA with microRNA-like functions. Mol Cell 32: 519–528.
38. Taft RJ, Glazov EA, Lassmann T, Hayashizaki Y, Carninci P, et al. (2009) Small RNAs derived from snoRNAs. RNA 15: 1233–1240.
39. Brameier M, Herwig A, Reinhardt R, Walter L, Gruber J (2010) Human box C/D snoRNAs with miRNA like functions: expanding the range of regulatory RNAs. Nucleic Acids Res 39: 675–686.
40. Mourtada-Maarabouni M, Pickard MR, Hedge VL, Farzaneh F, Williams GT (2009) GAS5, a non-protein-coding RNA, controls apoptosis and is downregulated in breast cancer. Oncogene 28: 195–208.
41. Mourtada-Maarabouni M, Hasan AM, Farzaneh F, Williams GT (2010) Inhibition of human T-cell proliferation by mammalian target of rapamycin (mTOR) antagonists requires noncoding RNA growth-arrest-specific transcript 5 (GAS5). Mol Pharmacol 78: 19–28.
42. Askarian-Amiri ME, Crawford J, French JD, Smart CE, Smith MA, et al. (2011) SNORD-host RNA Zfas1 is a regulator of mammary development and a potential marker for breast cancer. RNA 17: 878–891.
43. Asano M, Furukawa K, Kido M, Matsumoto S, Umesaki Y, et al. (1997) Growth retardation and early death of b-1,4-galactosyltransferase knockout mice with augmented proliferation and abnormal differentiation of epithelial cells. EMBO J 16: 1850–1857.
44. Hruz T, Wyss M, Docquier M, Pfaffl MW, Masanetz S, et al. (2011) RefGenes: identification of reliable and condition specific reference genes for RT-qPCR data normalization. BMC Genomics 12: 156. doi:10.1186/1471-2164-12-156.
45. Hirose T, Steitz J (2001) Position within the host intron is critical for efficient processing of box C/D snoRNAs in mammalian cells. Proc Natl Acad Sci USA 98: 12914–12919.

Hepatology Research

Hepatology Research 2014; 44: 460–473 doi: 10.1111/hepr.12140

Original Article

Cilostazol attenuates hepatic stellate cell activation and protects mice against carbon tetrachloride-induced liver fibrosis

Shunichi Saito,[1] Koichiro Hata,[1] Keiko Iwaisako,[1,3] Atsuko Yanagida,[1] Masatoshi Takeiri,[2] Hirokazu Tanaka,[1] Shoichi Kageyama,[1] Hirofumi Hirao,[1] Kazuo Ikeda,[3] Masataka Asagiri[2] and Shinji Uemoto[1]

[1]*Department of Surgery, Division of Hepato-Pancreato-Biliary Surgery and Transplantation, and* [2]*Innovation Center for Immunoregulation and Therapeutics, Graduate School of Medicine, Kyoto University, Kyoto, and* [3]*Department of Anatomy and Regenerative Biology, Graduate School of Medicine, Osaka City University, Osaka, Japan*

Aim: Liver fibrosis is a common pathway leading to cirrhosis. Cilostazol, a clinically available oral phosphodiesterase-3 inhibitor, has been shown to have antifibrotic potential in experimental non-alcoholic fatty liver disease. However, the detailed mechanisms of the antifibrotic effect and its efficacy in a different experimental model remain elusive.

Methods: Male C57BL/6J mice were assigned to five groups: mice fed a normal diet (groups 1 and 2); 0.1% or 0.3% cilostazol-containing diet (groups 3 and 4, respectively); and 0.125% clopidogrel-containing diet (group 5). Two weeks after feeding, groups 2–5 were intraperitoneally administered carbon tetrachloride (CCl_4) twice a week for 6 weeks, while group 1 was treated with the vehicle alone. To investigate the effects of cilostazol on hepatic cells, *in vitro* studies were conducted using primary hepatic stellate cells (HSC), Kupffer cells and hepatocytes with cilostazol supplementation.

Results: Sirius red staining revealed that groups 3 and 4 exhibited a lesser fibrotic area (2.49 ± 0.43% and 2.31 ± 0.30%, respectively) than group 2 (3.17 ± 0.67%, $P < 0.05$ and $P < 0.001$, respectively). *In vitro* studies showed cilostazol dose-dependently suppressed HSC activation (assessed by morphological change, cell proliferation, and the expression of HSC activation markers), suggesting the therapeutic effect of cilostazol is mediated by its direct action on HSC.

Conclusion: Cilostazol could alleviate CCl_4-induced hepatic fibrogenesis *in vivo*, presumably due, at least partly, to its direct effect to suppress HSC activation. Given its clinical availability and safety, it may be a novel therapeutic intervention for chronic liver diseases.

Key words: carbon tetrachloride, cilostazol, hepatic stellate cells, liver fibrosis, phosphodiesterase-3 inhibitor, platelet-derived growth factor

Correspondence: Dr Koichiro Hata, Department of Surgery, Division of Hepato-Pancreato-Biliary Surgery and Transplantation, Graduate School of Medicine, Kyoto University, Kyoto 606-8507, Japan.
Email: khata@kuhp.kyoto-u.ac.jp; Dr Masataka Asagiri, Innovation Center for Immunoregulation and Therapeutics, Graduate School of Medicine, Kyoto University, Kyoto 606-8501, Japan.
Email: masa-asagiri@umin.org

Conflict of interest: Drs Hata and Uemoto receive a grant from Otsuka Pharma. Dr Asagiri receives a grant from the AK Project (between Astellas Pharma and Kyoto University). However, the study was designed, conducted, analyzed, and reported independently of the funding agencies and pharmaceutical companies, although cilostazol was supplied by Otsuka Pharmaceutical. No other potential conflict of interest relevant to this article was reported.
Received 17 August 2012; revision 8 April 2013; accepted 15 April 2013.

INTRODUCTION

LIVER FIBROSIS, A precursor to cirrhosis, is a common consequence of almost all types of chronic liver injuries, including viral, alcoholic, autoimmune, metabolic and drug-induced liver diseases.[1] Fibrosis results from excessive accumulation of extracellular matrix (ECM) components, such as collagen type I. Left untreated, fibrosis can progress to liver cirrhosis and ultimately lead to organ failure and death. The activation of hepatic stellate cells (HSC) in response to liver injury is considered to be an essential event underlying hepatic fibrogenesis.[2–4] The activation of HSC refers to the trans-differentiation of quiescent HSC into proliferative and contractile myofibroblast-like cells. These activated HSC

secrete excess ECM proteins and contribute to the development of hepatic fibrosis. Several types of growth factors, cytokines, chemokines and their cognate receptors are associated with HSC activation. Among these, transforming growth factor (TGF)-β1 and platelet-derived growth factor (PDGF) are probably the most important.[5–7] HSC play a key role in liver fibrosis, thereby restraining the activation of HSC may attenuate liver fibrosis. Thus, numerous studies have attempted to suppress HSC activation in order to develop new treatment strategies for hepatic fibrosis.[8–11] Cilostazol (OPC-13013 [6-[4-[1-cyclohexyl-1H-tetrazol-5-yl]butoxy]-3,4-dihydro-2[1H]-quinolinone]) is a synthetic vasodilator and an antiplatelet agent. It was approved in 1988 in Japan for the treatment of symptoms related to occlusive peripheral arterial disease (Pletaal; Otsuka Pharmaceutical Co., Ltd., Tokyo, Japan) and subsequently in 1999 in the USA and in 2001 in the UK (Pletal; Otsuka America Pharmaceutical, Inc., Rockville, MD, USA and Otsuka Pharmaceutical Europe Ltd., Uxbridge, UK) for the treatment of intermittent claudication symptoms.[12–14] Over the past 20 years, it has been widely used as a potent inhibitor of platelet aggregation and thrombosis.[15–18] It has also been shown to inhibit PDGF secretion *in vitro*.[19] The antiplatelet activity of cilostazol is attributed to its inhibition of cyclic adenosine monophosphate (cAMP) phosphodiesterase (PDE). Recent studies have identified 11 different families of PDE. Of these, cilostazol selectively inhibits PDE3, which is predominantly expressed in platelets, vascular smooth muscle cells, cardiac myocytes and hepatic cells.[20,21] Recently, increased intracellular cAMP has been shown to inhibit HSC activation,[22–25] although little is known about the effect of cilostazol on liver fibrosis. Furthermore, cilostazol was shown to have an antifibrotic potential in experimental non-alcoholic fatty liver disease.[26] However, the precise mechanisms of the antifibrotic effect and its efficacy in a different experimental model are elusive. This study was designed to investigate the effect of cilostazol on carbon tetrachloride (CCl_4)-induced hepatic fibrogenesis in mice and to clarify its mechanism of action by pathological examination and analysis of primary cells derived from the mice.

METHODS

Animals

MALE C57BL/6J MICE aged 4 weeks were purchased from Japan SLC (Shizuoka, Japan). After an acclimation period of 7 days, the mice were randomly assigned to the five treatment groups ($n = 10$ per group) in a single-blinded fashion (Fig. 1). The mice were maintained on standard chow and allowed free access to food and water. The protocol for animal handling was reviewed and approved by the Animal Care and Use Committee of Kyoto University.

Mouse model of liver fibrosis

Two weeks after assignment to treatment groups, the mice were treated with CCl_4 (2 μL/g bodyweight diluted 1:4 in corn oil) by intraperitoneal (i.p.) injection twice a week for 6 weeks. The mice were sacrificed 4 days after the last injection.

Drugs and drug treatment

The antiplatelet drug cilostazol was a gift from Otsuka Pharma (Tokushima, Japan). Clopidogrel was purchased from Sanofi-Aventis (Tokyo, Japan). Each drug was administrated in standard pellet food (Oriental Bio Service, Kyoto, Japan) containing cilostazol (0.1% w/w), cilostazol (0.3% w/w) or clopidogrel (0.125% w/w). Oral treatment with cilostazol at 0.1% and 0.3% w/w, and clopidogrel at 0.125% w/w of chow is equivalent to the clinically used doses.[27–29] The alternative antiplatelet drug clopidogrel was used as a control. To raise and stabilize the plasma concentration of the drugs, the animals were pretreated with the drugs for 2 weeks. All animals were closely observed for 2 weeks after the dietary change, and then received CCl_4 injections for 6 weeks. The food intake and bodyweight changes were monitored throughout the experimental period for 8 weeks. Blood samples were collected from the inferior vena cava of the mice, and liver weights were recorded at death.

Histological examination and immunohistochemistry

For histological evaluation, the right lobe of the liver of each mouse was collected at death and fixed in 4% paraformaldehyde (PFA). In order to assess fibrosis, paraffin-embedded sections were stained with picrosirius red (Sigma, St Louis, MO, USA).[30] Expression levels of α-smooth muscle actin (α-SMA) and F4/80 were immunohistochemically determined in paraffin-embedded sections as described previously[31] using a monoclonal antimouse α-SMA antibody (1:300, clone: 1A4; Dako, Glostrup, Denmark) or anti-mouse F4/80 antibody (1:100, clone: BM8; eBioscience, San Diego, CA, USA), respectively.

Sirius red-positive areas, α-SMA-positive areas and F4/80-positive areas were quantified from 10 random ×100 fields from each animal ($n = 10$ per treatment

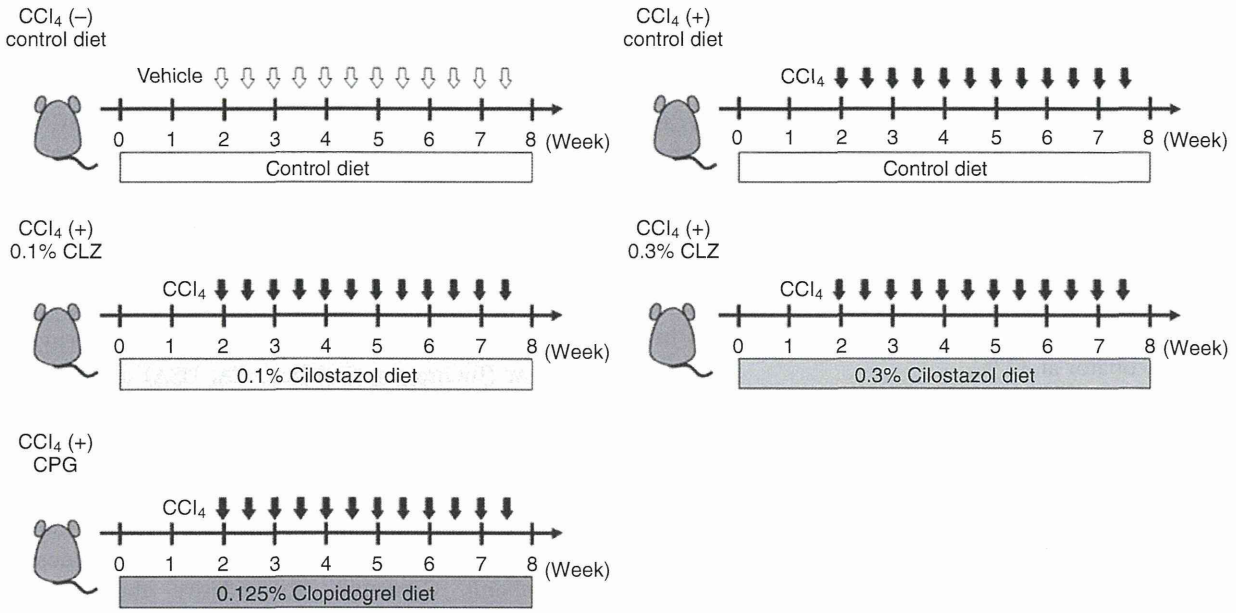

Figure 1 Experimental protocol. Male adult C57BL/6J mice were fed pelleted food containing 0.1% or 0.3% cilostazol or 0.125% clopidogrel, or fed a control diet. Liver fibrosis was induced by i.p. injection of CCl_4 twice a week for 6 weeks. Mice were killed 4 days after the last injection. CLZ, cilostazol; CPG, clopidogrel; CCl_4, carbon tetrachloride. ($n = 10$). ⇩, vehicle i.p.; ⬇, CCl_4, 0.5 μL/g bodyweight i.p.

group) using image processing software (BZ analyzer; Keyence, Osaka, Japan). Data are presented as the percentage area positively stained for Sirius red, α-SMA or F4/80.

Measurement of hepatic collagen content

For measurement of liver fibrosis, the specific amino acid of collagen type I, hydroxyproline, was quantified in liver tissue. The hepatic hydroxyproline content was measured as previously described.[32] In brief, liver tissue was homogenized in 900 μL of ice-cold distilled water. Subsequently, 125 μL of 50% trichloroacetic acid was added, and the homogenates were incubated on ice for 20 min. Precipitated pellets were hydrolyzed for 18 h at 110°C in 6 N HCl. After hydrolysis, the samples were filtered and neutralized with 10 N NaOH, and hydrolysates were oxidized with chloramine-T (Sigma) for 25 min at room temperature. The reaction mixture was then incubated in Ehrlich's perchloric acid solution at 65°C for 20 min and then cooled to room temperature. Sample absorbance was measured at 560 nm in duplicate. Purified hydroxyproline (Sigma) was used as a standard. The hydroxyproline content was expressed as nanograms of hydroxyproline per gram of liver.

Immunoblot analysis

For analysis of α-SMA protein expression, immunoblotting was performed with whole liver lysates (20 μg/lane) using standard techniques. Immunoblotting was performed using a polyclonal antigoat glyceraldehyde 3-phosphate dehydrogenase (GAPDH) antibody (1:200; #sc-20357; Santa Cruz Biotechnology, Santa Cruz, CA, USA) as an internal control, a polyclonal antirabbit α-SMA antibody (1:200; #ab-5694; Abcam, Cambridge, UK) and horseradish peroxidase-conjugated secondary antibodies (Santa Cruz Biotechnology) as described in the manufacturer's protocol.[33] Antibody staining was visualized with an enhanced chemiluminescence system (GE Healthcare Biosciences, Little Chalfont, UK) using Lumino-image analyzer (LAS-3000 mini; Fujifilm, Tokyo, Japan). Band density was quantified from digital images using ImageJ software.

Isolation and culture of hepatic cells

Primary HSC, Kupffer cells and hepatocytes were isolated from the mouse liver as described previously.[34–36] In brief, HSC and Kupffer cells were isolated from mice by two-step collagenase–pronase perfusion followed by three-layer discontinuous density gradient

centrifugation with 8.2% (w/v) and 14.5% (w/v) Nycodenz (Accurate Chemical and Scientific, Westbury, NY, USA) to obtain HSC and Kupffer cell fractions. HSC were collected between the 0% and 8.2% (w/v) layer. Kupffer cells were collected between the 8.2% and 14.5% (w/v) layers and purified by differential plating. HSC and Kupffer cells were cultured in Dulbecco's modified Eagle's medium (DMEM; Sigma) supplemented with 10% fetal bovine serum (FBS) and antibiotics. Hepatocytes were cultured in William's medium E supplemented with 10% FBS and antibiotics on the collagen-coated dish. Hepatic cells were cultured in a CO_2 incubator at 37°C.

Cilostazol treatment

Cilostazol was dissolved in dimethylsulfoxide and diluted in DMEM supplemented with 10% FBS and antibiotics. Complete medium containing final concentration of 0 μM (control), 5 μM and 15 μM cilostazol was added to cultures 1 day after isolation.

Measurement of Intracellular cAMP

The intracellular cAMP level was measured as described previously[37] using the cAMP-Glo max assay kit (Promega, Madison, WI, USA). Briefly, 1×10^4 cells were seeded in a 96-well plate with or without cilostazol in culture medium containing 10% FBS and incubated at 37°C for 24 h. The cAMP detecting solution was added to each well and incubated at room temperature for 20 min. The Kinase-Glo reagent was added to each well. The plate was shaken for 1 min at room temperature and incubated at room temperature for 10 min. Finally, the luminescent signal was measured by a plate reader (Arvo; Perkin-Elmer, Waltham, MA, USA).

Time-lapse recording and cell counting

For the observation of morphological changes, HSC were placed in a Lab-Tek plastic four-well chamber slide (Nunc, Naperville, IL, USA) and maintained at 37°C in 10% CO_2. Time-lapse images were taken using an inverted microscope (BZ9000; Keyence, Osaka, Japan) over 6 days following cilostazol treatment. Cells were counted in four random ×200 fields on each chamber using BZ analyzer image processing software.

Cytochemical analysis

Primary HSC in each chamber were fixed in 10% formalin/PBS for 10 min blocked with Dako Protein Block (#X0909; Dako, Glostrup, Denmark) for 1 h, incubated overnight with a polyclonal antimouse α-SMA antibody (1:200; #A2524, Sigma) in a blocking solution, washed with PBS, and incubated with Alexa Flour 594 goat antimouse immunoglobulin G (1:600; #A-11005; Invitrogen, San Diego, CA, USA) secondary antibody and 4′,6′-diamidino-2-phenylindole dihydrochloride (DAPI) nuclear stain for 1 h. Finally, HSC were washed and observed with an inverted fluorescence microscope, BZ9000 (Keyence).

Reverse-transcriptase quantitative polymerase chain reaction (RT–qPCR)

For gene expression analysis, total RNA was extracted from liver tissue, HSC or Kupffer cells using TRIZOL reagent (Invitrogen, Carlsbad, CA, USA) according to the manufacturer's protocol. DNase-treated RNA was reverse transcribed using the Omniscript RT Kit (Qiagen, Hilden, Germany) according to the manufacturer's protocol. RT-qPCR was performed for 55 cycles of 15 s at 95°C and 60 s at 60°C using SYBR Green I Kits for the LightCycler 480 instrument (Roche Diagnostics, Mannheim, Germany). The relative abundance of target genes was calculated using a standard curve normalized to α-tubulin or 18S. Probes and primers for α-SMA (NM_007392), collagen α1 (I) (NM_007742), PDGF-B (NM_011057), PDGF receptor (PDGFR)-β (NM_008809), TGF-β1 (NM_011577), TGF-βR1 (NM_009370), tumor necrosis factor (TNF)-α (NM_013693), interleukin (IL)-1β (NM_008361), monocyte chemotactic protein (MCP)1 (NM_011333), F4/80 (NM_010130), 18S (NR_003278) and α-tubulin (NM_011653) were designed by and purchased from Life Technologies (Carlsbad, CA, USA).

Statistical analysis

Results are reported as mean ± 95% confidence intervals (CI). Statistical comparisons were made using Student *t*-test or two- or one-way ANOVA followed by Bonferroni's post-hoc test. $P < 0.05$ was considered to be significant.

RESULTS

Cilostazol alleviated fibrous change in the liver

IN ORDER TO validate the antifibrotic efficacy of cilostazol, we utilized a widely used experimental mouse model of liver fibrosis induced by CCl_4 injections (twice a week for 6 weeks; Fig. 1). Based on the pharmacokinetic data of the plasma concentration of the drugs, 0.1% and 0.3% cilostazol and 0.125% clopidogrel were used as clinically equivalent doses. Collagen deposition, a marker for liver fibrosis, was assessed by Sirius red

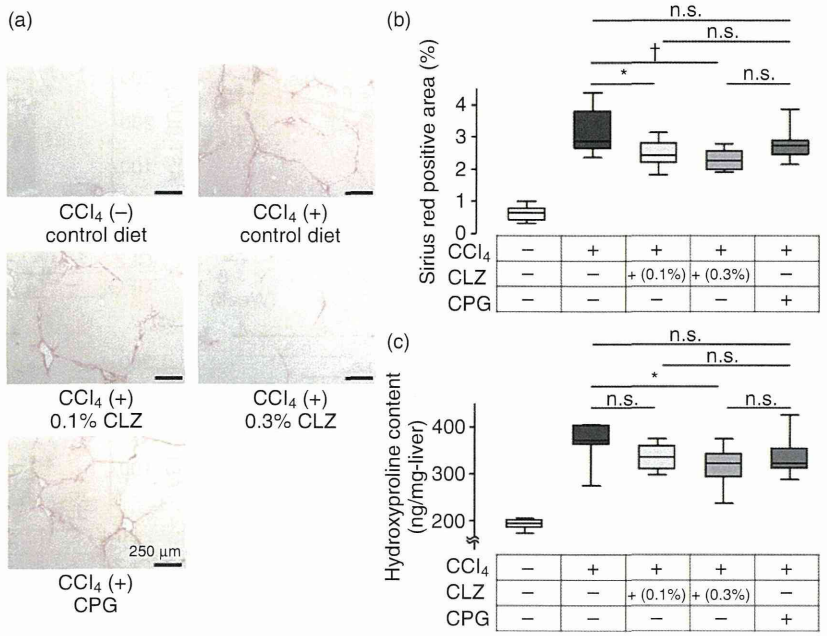

Figure 2 Cilostazol alleviated fibrous changes in the liver. (a) Sirius red staining of liver sections in each group. CCl_4 treatment for 6 weeks remarkably increased the fibrotic area. CCl_4-treated liver in the control or clopidogrel-administrated group showed bridging fibrosis. Cilostazol decreased the fibrotic area among CCl_4-treated mice (original magnification ×100). (b) Quantification of liver fibrosis area stained by Sirius red. CCl_4-induced fibrous areas in the 0.1% or 0.3% cilostazol-administrated groups were significantly decreased compared with that in the control group. (c) Hydroxyproline assay was performed to measure the total collagen content. Administration with 0.3% cilostazol reduced tissue hydroxyproline levels compared with control. The box plots present the median and 25th–75th percentiles. Upper and lower lines represent the minimum and maximum values ($n = 10$). $^*P < 0.05$; $\dagger P < 0.001$ vs CCl_4-treated control. CCl_4, carbon tetrachloride; CLZ, cilostazol; CPG, clopidogrel.

staining (Fig. 2a). Sirius red staining of the liver in the 0.1% and 0.3% cilostazol-administrated groups (2.49%; 95% CI = 2.18–2.80; and 2.31%; 95% CI = 2.10–2.52) was significantly lower than in the control group (3.17%; 95% CI = 2.70–3.65; $P < 0.05$ and $P < 0.001$, respectively), however, clopidogrel had no effect (Fig. 2a,b). This was reflected by hydroxyproline content, which was significantly reduced in the 0.3% cilostazol-administrated group (317 ng/mg liver; 95% CI = 289–346) compared with that in the control group (371 ng/mg liver; 95% CI = 344–398; $P < 0.001$; Fig. 2c). Thus, p.o. administration of cilostazol reduces hepatic fibrogenesis at clinical doses. During the 8-week experimental duration, no significant difference in bodyweight change or peripheral platelet count was observed among treatment groups (Fig. 3a,b), indicating minimal toxicity of the drugs. Moreover, there was no apparent difference in CCl_4-induced hepatocyte damage among the groups, as assessed by peripheral blood aspartate aminotransferase and alanine aminotransferase levels (Fig. 3c,d) and hematoxylin–eosin staining (Fig. 3e). We also observed no morphological change in cultured primary hepatocytes supplemented with cilostazol (Fig. 3f).

Cilostazol attenuated the activation of HSC in the liver

Chronic liver injury can lead to unrestrained HSC activation, resulting in excessive production of extracellular matrices and hepatic fibrosis. Thus, we assessed the activation status of HSC in the liver, by immunohistochemical staining of α-SMA, a marker of HSC activation (Fig. 4a). Similar to the Sirius red staining data, the α-SMA positive area in the liver of the 0.1% (4.16%; 95% CI = 3.17–5.15) and 0.3% (2.61%; 95% CI = 2.17–3.05) cilostazol-administrated groups was clearly reduced in a dose-dependent manner compared with the control group (7.13%; 95% CI = 4.10–10.2; $P < 0.05$ and $P < 0.001$, respectively; Fig. 4b) and clopidogrel-administrated animals. This result was also reflected by immunoblotting experiments in which α-SMA protein expression was significantly reduced in

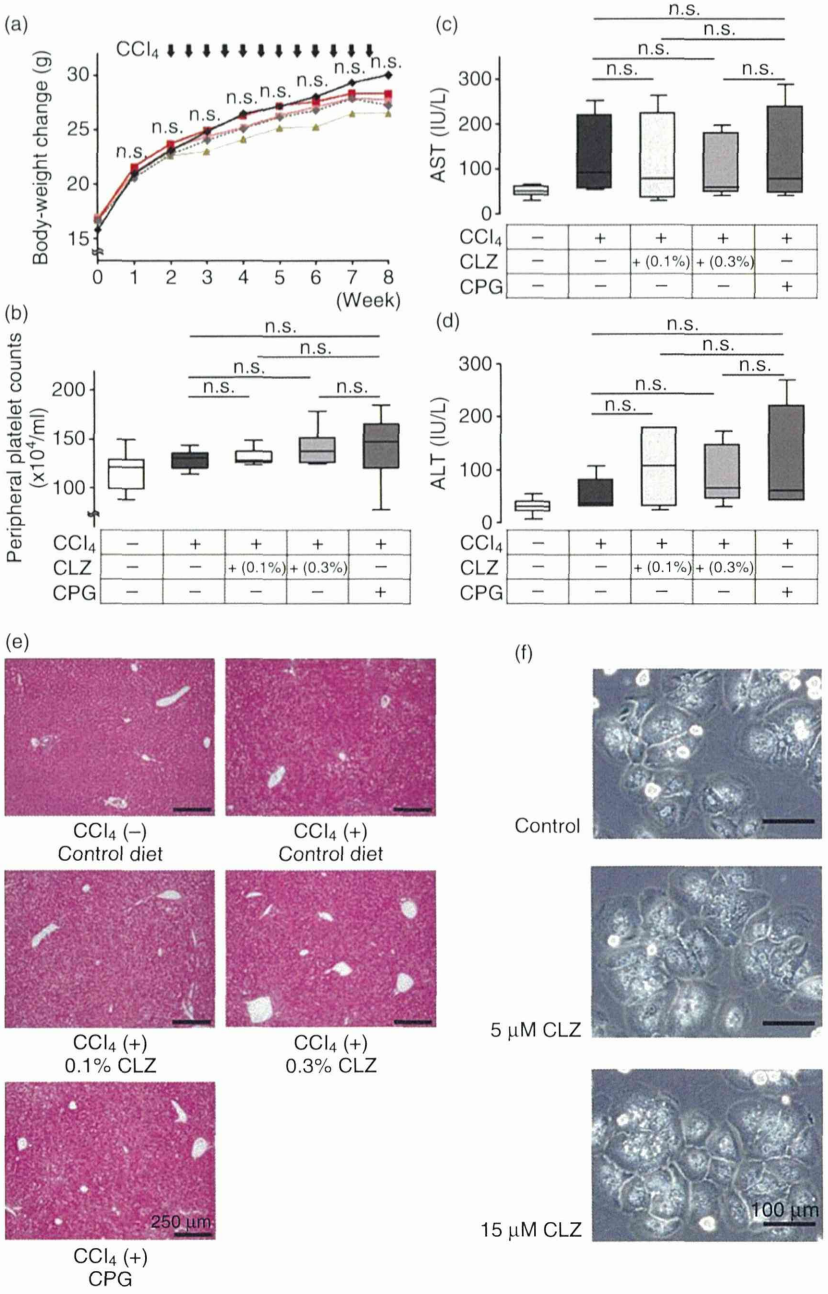

Figure 3 Bodyweight change, peripheral platelet counts, hepatocyte damage and aspartate aminotransferase (AST)/alanine aminotransferase (ALT) did not differ among the CCl_4-treated groups. (a) Bodyweight change during the 8-week experimental duration. Mice without CCl_4 treatment showed the highest gain, however, no significant differences were observed among groups. (b) Peripheral platelet counts at death were not different among CCl_4-treated groups. (c,d) Serum AST and ALT levels at death were not different among CCl_4-treated groups. (e) Hematoxylin–eosin staining of liver sections from each group (original magnification ×100). No obvious differences in hepatocyte damage existed among CCl_4-treated groups. (f) Morphology of hepatocytes supplemented with cilostazol for 1 day was observed under a phase contrast microscope (original magnification ×200). The morphology was unaffected by cilostazol supplementation. On line plots, each plot represents the mean of measurements ($n = 10$). The box plots present the median and 25th–75th percentiles. Upper and lower lines represent the minimum and maximum values ($n = 10$). CCl_4, carbon tetrachloride; CLZ, cilostazol; CPG, clopidogrel. ◆—, CCl_4 (–) + control diet; ■—, CCl_4 (+) + 0.3% cilostazol; ■—, CCl_4 (+) + 0.1% cilostazol; ◆—, CCl_4 (+) + control diet; ▲—, CCl_4 (+) + clopidogrel.

the 0.3% cilostazol-administrated group (0.44%; 95% CI = 0.29–0.60) compared with that in the control group (1.14%; 95% CI = 0.55–1.72; $P < 0.05$; Fig. 4c). These results indicate that cilostazol has potent activity to attenuate HSC activation in the liver through unknown mechanisms.

Cilostazol directly and effectively inhibits the activation of HSC but not of Kupffer cells

To reveal the possible mechanisms underlying these *in vivo* observations, we performed *in vitro* studies in

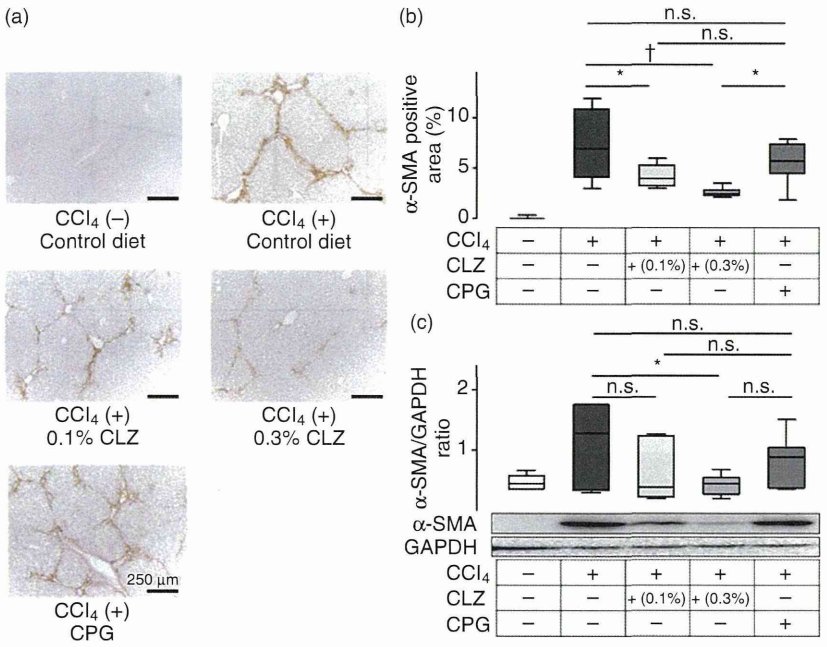

Figure 4 Cilostazol attenuated the expression of α-SMA protein in the liver. (a) α-SMA immunostaining of liver sections in each group. Treatment with CCl_4 for six weeks remarkably increased α-SMA expression. Among CCl_4-treated groups, the liver in cilostazol-administrated groups has a reduced α-SMA-positive area compared with that in the control diet or clopidogrel-administrated group (original magnification ×100). (b) Quantification of the α-SMA positive area in each group. Cilostazol-administrated groups had significantly decreased α-SMA positive areas compared with control diet and clopidogrel-administrated groups. (c) Measurement of α-SMA protein in the liver by immunoblotting. Administration of 0.3% cilostazol reduced α-SMA levels in CCl_4-treated mice. The box plots present the median and 25th–75th percentiles. Upper and lower lines represent the minimum and maximum values ($n = 10$). $^*P < 0.05$; $\dagger P < 0.001$ vs CCl_4-treated control diet group. α-SMA, α-smooth muscle actin; CCl_4, carbon tetrachloride; CLZ, cilostazol; CPG, clopidogrel; GAPDH, glyceraldehyde 3-phosphate dehydrogenase.

primary cultures of HSC. Generally, isolated HSC undergo autonomous activation in culture, and the activation is associated with a depletion of retinoid droplets, morphological change, cell proliferation, and expression of several activation markers such as α-SMA and collagen α1 (I). During 6 days of culture, control HSC gradually lost retinoid droplets and showed myofibroblast-like activated morphology, whereas cilostazol-supplemented HSC maintained retinoid droplets and retained quiescent morphology (Fig. 5a). In addition, cilostazol suppressed HSC proliferation in a dose-dependent manner, without showing cell toxicity (Fig. 5b). The expression of α-SMA protein was dose-dependently suppressed in the presence of cilostazol (Fig. 5c). Because Kupffer cells have been shown to be implicated in liver fibrosis as well as HSC,[11,38–40] we examined the effect of cilostazol on Kupffer-cell activation *in vivo* and *in vitro*. Pathological examination revealed a weak tendency for decrease in the F4/80 positive (Kupffer cell) area in the liver of cilostazol-administrated mice, however, we could not detect significant changes in our experimental setting (Fig. 5d,e), and no significant change was observed in mRNA levels of tissue TNF-α and TGF-β1 in the liver by cilostazol treatment (Fig. 5f). In fact, cilostazol did not affect the mRNA expression of F4/80 in isolated Kupffer cells (Fig. 5g), suggesting the minimal effect of cilostazol *in vivo* may be simply explained by the secondary effect of the resolution of fibrosis. Likewise, cilostazol exhibited an insignificant effect on the Kupffer cell production of TNF-α, IL-1β, MCP1 and TGF-β1 (Fig. 5g). These data together propose the notion that the *in vivo* therapeutic efficacy of cilostazol is mediated, at least in part, by its direct effects on HSC. If so, why did HSC respond well to cilostazol? One possible explanation is that HSC are more sensitive to cilostazol than other cell types (e.g., Kupffer cells). Actually, cilostazol-induced cAMP accumulation, which is an indicator for cilostazol

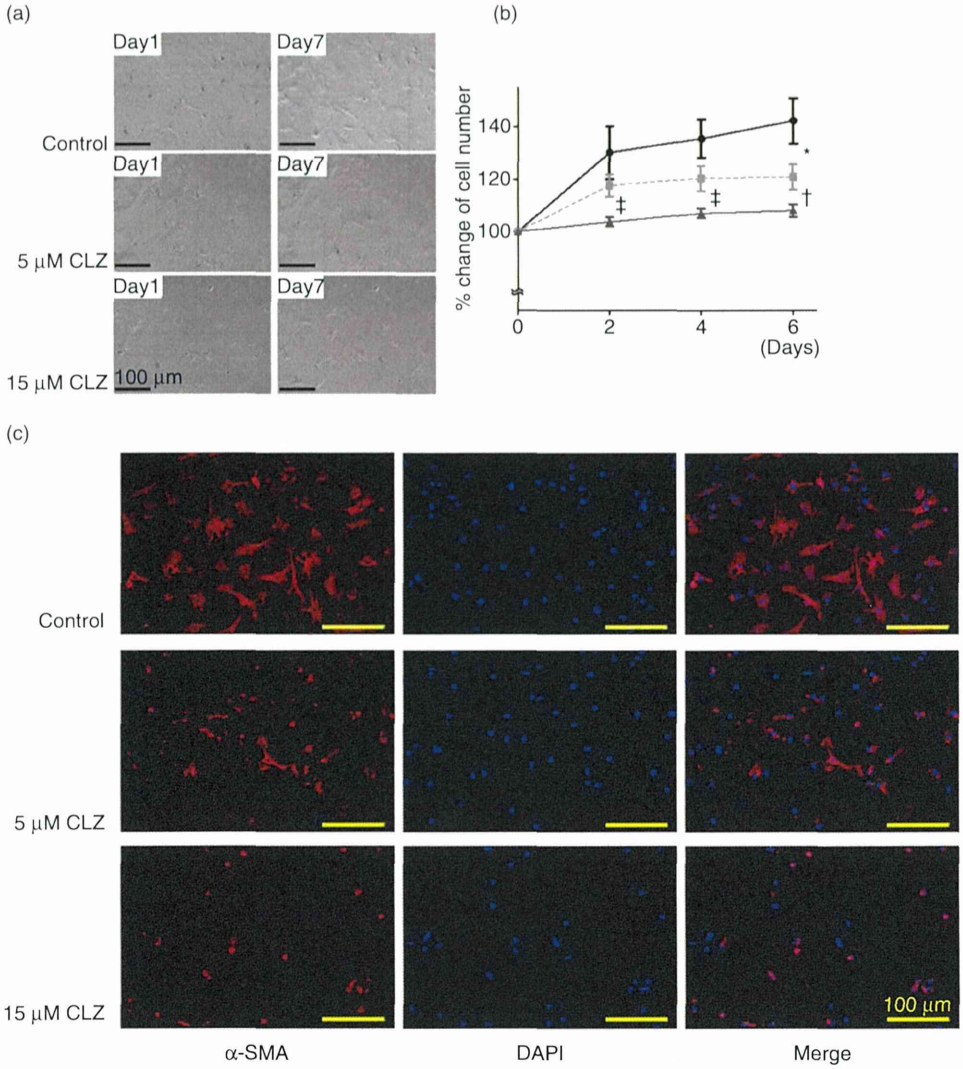

Figure 5 Cilostazol suppressed the proliferation and activation of HSC, but did not affect Kupffer-cell activation. (a) Morphological changes in HSC from 0–6 days were viewed on a phase contrast microscope (original magnification ×200). HSC supplemented with 15 μM cilostazol resulted in visible short cytoplasmic dendritic processes and perinuclear vacuoles containing retinoids. (b) HSC proliferation was determined by direct count of the cell numbers. Cilostazol supplementation slowed the increase in cell numbers compared with control. (c) Immunofluorescent staining of α-SMA (red) in HSC on the second day of culture (original magnification ×200). The protein expression of α-SMA was decreased in cilostazol-supplemented HSC in a dose-dependent manner. (d) F4/80 immunostaining of liver sections in each group. (original magnification ×100). (e) Quantification of the F4/80-positive area in each group. Cilostazol-administrated groups tended to show fewer F4/80-positive areas than the control, but no significant differences were observed among CCl_4-treated groups. (f) mRNA expression levels of TNF-α and TGF-β1 in the liver were not affected by cilostazol. (g) Expression of Kupffer cell marker (F4/80) and inflammation-related genes (TNF-α, IL-1β, MCP1 and TGF-β1) in primary Kupffer cells on the second day of culture was not altered by cilostazol. (h) Accumulation of cAMP in primary cultured HSC and Kupffer cells. Cilostazol supplementation significantly elevated the cAMP level only in HSC. The box plots present the median and 25th–75th percentiles. Upper and lower lines represent the minimum and maximum values ($n = 4$). *$P < 0.05$; †$P < 0.001$; ‡$P < 0.01$ vs control group. α-SMA, α-smooth muscle actin; cAMP, cyclic adenosine monophosphate; CCl_4, carbon tetrachloride; CLZ, cilostazol; DAPI, 4′,6′-diamidino-2-phenylindole dihydrochloride; HSC, hepatic stellate cell; IL-1β, interleukin-1β; MCP1, monocyte chemotactic protein-1; TNF-α, tumor necrosis factor-α; TGF-β1, transforming growth factor-β1. —●—, control; - -■- -, 5 μM CLZ; —▲—, 15 μM CLZ.

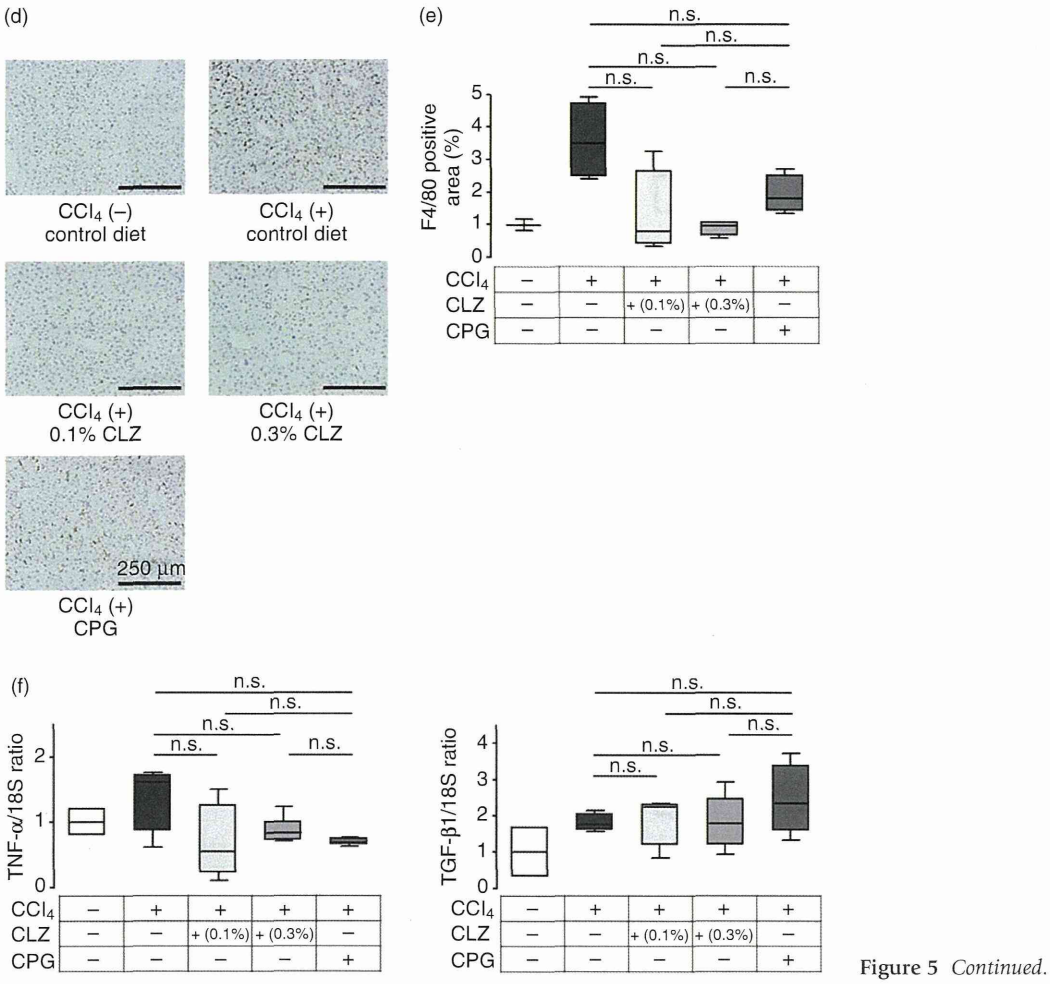

Figure 5 *Continued.*

inhibition of the PDE3 enzyme, was significantly higher only in HSC supplemented with cilostazol (2.283; 95% CI = 1.45–3.12; $P < 0.01$) but not in Kupffer cells (1.363; 95% CI = 0.4374–2.289; Fig. 5 h).

Cilostazol suppressed PDGFR expression in HSC

To further delineate the effect of cilostazol on the activation of HSC, we characterized the cilostazol-affected gene expression profiles during the activation phase of HSC. First, to confirm the direct effects of cilostazol on the gene activation mechanism of HSC, we examined the α-SMA and collagen α1 (I) gene induction. As suggested by the previous data (Figs 2,4,5), mRNA induction of α-SMA was lower in cells supplemented with 5 μM cilostazol (0.555; 95% CI = 0.085–1.024) and 15 μM cilostazol (0.221; 95% CI = 0.086–0.356) when compared with the control (2.53; 95% CI = 1.01–4.05; $P < 0.01$; Fig. 6a). Similarly, collagen α1 (I) mRNA expression was lower in cells supplemented with 5 μM cilostazol (0.411; 95% CI = 0.010–0.833) and 15 μM cilostazol (0.059; 95% CI = 0.042–0.159) as compared with the control cells (2.20; 95% CI = 0.31–4.08; $P < 0.01$; Fig. 6b). Then, to gain further mechanistic insight into the action of cilostazol on HSC, the mRNA expression of PDGF-B, PDGFR-β and TGF-βR1, an important cytokine and cytokine receptors for HSC activation, was determined. The expression of PDGF-B, one of the most important mitogens for HSC, was unaffected by cilostazol treatment (Fig. 6c), however, PDGFR-β mRNA expression in the 5 μM cilostazol-supplemented cells (0.282; 95% CI = 0.104–0.460) and

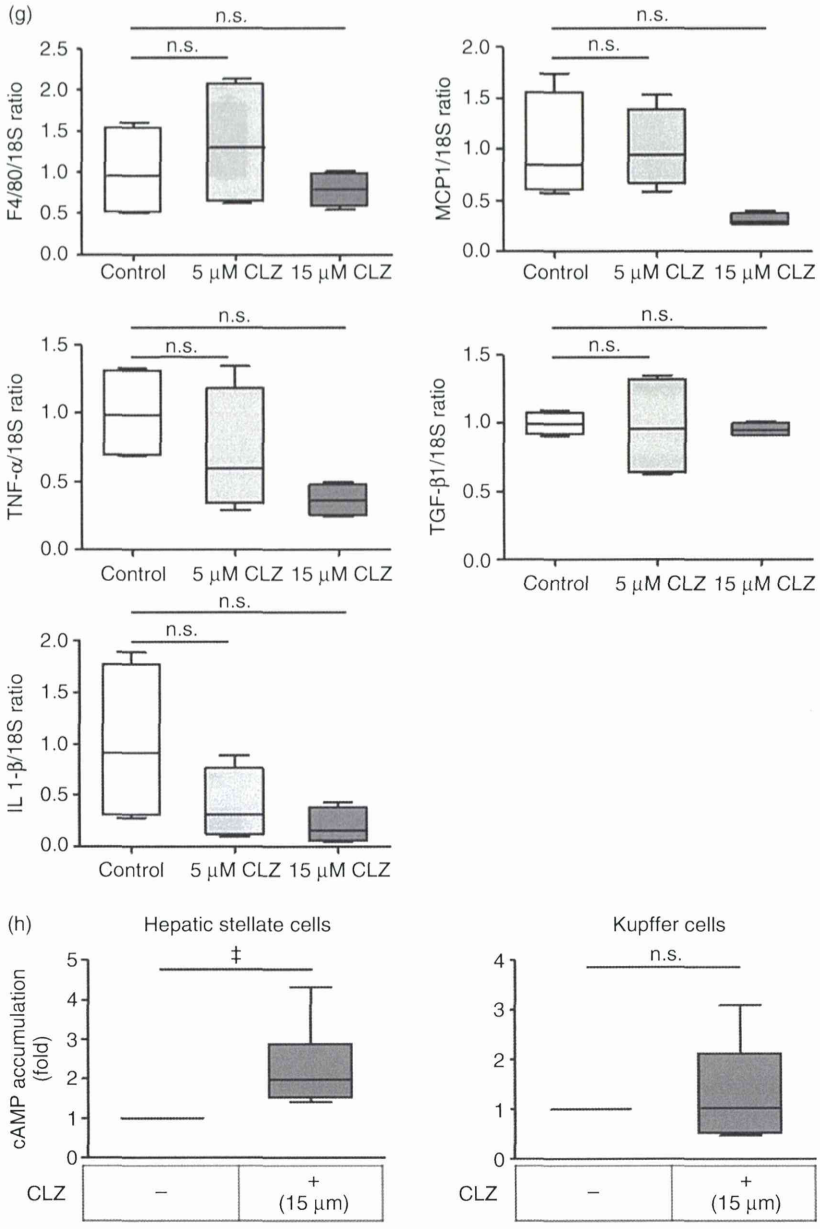

Figure 5 *Continued.*

15 μM cilostazol-supplemented cells (0.336; 95% CI = 0.036–0.636) was significantly decreased compared with that in control cells (0.749; 95% CI = 0.290–1.210; $P < 0.001$; Fig. 6d). In contrast, TGF-βR1 mRNA expression was not affected by cilostazol treatment (Fig. 6e). These results indicate the possibility that cilostazol attenuates the activation-induced proliferation of HSC through the abrogation of PDGF–autocrine signaling by limiting the receptor (PDGFR-β) signaling regardless of the ligand (PDGF) availability.

DISCUSSION

THE P.O. ADMINISTRATION of cilostazol effectively prevents the development of CCl_4-induced liver fibrosis in mice. In agreement with the previous study,

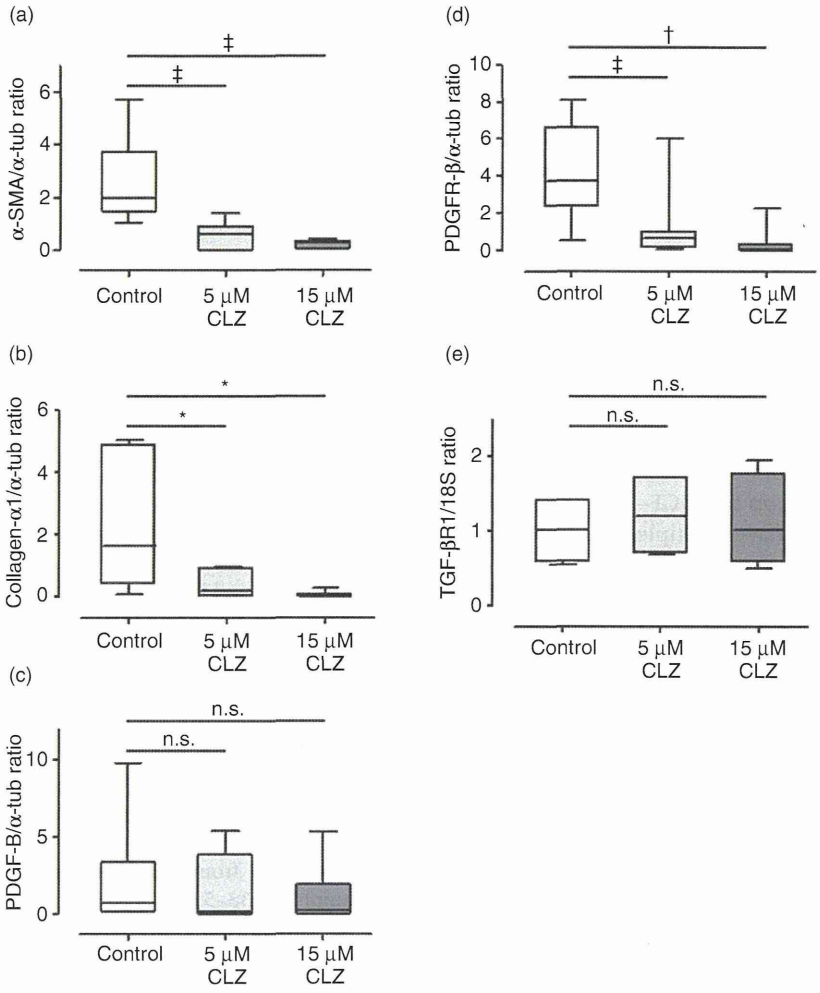

Figure 6 Expression of genes associated with HSC activation was assessed by reverse transcription quantitative polymerase chain reaction. (a) α-SMA, (b) collagen α1 (I) and (d) PDGFR-β expression levels in HSC supplemented with 5 μM and 15 μM cilostazol for 2 days were significantly suppressed compared with control (*$P < 0.05$; ‡$P < 0.01$; †$P < 0.001$ vs control, respectively). The expression of (c) PDGF-B and (e) TGF-βR1 had no difference between control and cilostazol-supplemented HSC. The box plots present the median and 25th–75th percentiles. Upper and lower lines represent the minimum and maximum values ($n = 7$). α-SMA, α-smooth muscle actin; CLZ, cilostazol; HSC, hepatic stellate cell; PDGF-B, platelet growth factor-B; PDGFR-β, platelet growth factor receptor-β; TGF-βR1, transforming growth factor-β receptor 1.

cilostazol was not toxic to HSC as indicated by the morphology and proliferation of the cells (Fig. 5a,b).[25] It is noteworthy that unlike many other candidate medications, cilostazol is already widely used as an antiplatelet agent in clinical practice with proven long-term safety. For this reason, cilostazol holds potential to become an antifibrotic agent for chronic liver diseases in humans.

In the present study, we employed clopidogrel as an alternative antiplatelet agent for the comparison. Although both cilostazol and clopidogrel showed minimal side-effects (Fig. 3), only cilostazol attenuated liver fibrosis (Figs 2,4), suggesting that cilostazol may have distinct antifibrotic mechanisms apart from its antiplatelet action. This notion is consistent with the results of the present *in vitro* study in which the treatment of primary HSC with cilostazol attenuated the HSC proliferation (Fig. 5b) and the expression of α-SMA and collagen α1 (I) (Figs 5c,6), indicating the direct effect of cilostazol on HSC. On the other hand, our *in vitro* and *in vivo* studies showed only a minimal effect of cilostazol on Kupffer cells (Fig. 5d,e,g,h), and no significant change was detected in inflammatory and fibrogenic genes (such as TNF-α and TGF-β1) by cilostazol administration (Fig. 5f). These results lend support to the concept that cilostazol exerts its antifibrotic effect(s) via the suppression of HSC activation *in vivo*.

As reported,[6,39,41] PDGFR-β was absent in quiescent HSC, but was upregulated in an early stage of liver injury. Activating factors from autocrine or paracrine sources such as TGF-β1 stimulate the transcriptional induction of PDGFR-β in quiescent HSC, thereby

rendering them responsive to PDGF-B chain molecules. Among several activating pathways, the autocrine loop exerted by PDGF–PDGFR signaling is regarded as one of the most potent mitogenic pathways for HSC.[42] Although PDGF itself seemed unaffected in our study, our quantitative analyses showed that cilostazol significantly suppressed PDGFR-β in HSC (Fig. 6c,d). Because the PDGF–PDGFR signaling not only promotes myofibroblast proliferation but also participates in other fibrogenic actions, including stimulation of collagen production and promotion of cell adhesion, it has been speculated that the activated PDGF–PDGFR signaling pathway is a candidate target for antifibrotic therapy in liver diseases.[43] Indeed, focusing on PDGFR, recent studies have shown attenuation of hepatic fibrosis by a PDGFR tyrosine kinase inhibitor.[44–46] In the same sense, a blockade of the autocrine loop of PDGF–PDGFR signaling by cilostazol may also have multiple benefits for preventing the development of hepatic fibrosis.

Cilostazol is a selective inhibitor of PDE3, and PDE3 inhibition in platelets exhibits antithrombotic effects by preventing platelet aggregation. Recently, increased intracellular cAMP levels and activation of protein kinase A (PKA) were reported to reduce PDGF-stimulated cellular proliferation.[47,48] Interestingly, cilostazol has been shown to be effective against the development of non-alcoholic fatty liver disease through the activation of the cAMP/PKA signaling pathway *in vivo*.[26] Although the exact mechanism remains to be determined, there may be a link between PDGFR downregulation and cAMP/PKA signaling in HSC.

In conclusion, orally bioavailable cilostazol attenuates HSC activation, possibly through the suppression of PDGFR expression in HSC, and thereby alleviates hepatic fibrogenesis. Further studies may yield a future intervention strategy against liver diseases.

ACKNOWLEDGMENTS

WE ARE GRATEFUL for technical assistance provided by the Central Laboratory of Osaka City University Medical School. We also thank Kimie Takafuji (Hamanaka), Eri Hikawa, Tadashi Mizutani, Kenta Aohara, Kazushi Yamasato and Marika Horiuchi. This work was supported in part by a Grant-in-Aid for Scientific Research (Grant Numbers 20372435 [M. A.], 21689035 [K. H.], 24689056 [M. A.]) from the Japan Society for the Promotion of Science; a grant from the Japanese Ministry of Health, Labour and Welfare (K. Iwaisako., K. Ikeda, M. A and S. U.); and grants from Otsuka Pharma (K. H and S. U.), the Uehara Memorial Foundation (M. A.) and Kanae Foundation for the Promotion of Medical Science (M. A.).

REFERENCES

1 Friedman SL. Mechanisms of hepatic fibrogenesis. *Gastroenterology* 2008; **134**: 1655–69.
2 Gabele E, Brenner DA, Rippe RA. Liver fibrosis: signals leading to the amplification of the fibrogenic hepatic stellate cell. *Front Biosci* 2003; **8**: d69–77.
3 Afdhal NH, Nunes D. Evaluation of liver fibrosis: a concise review. *Am J Gastroenterol* 2004; **99**: 1160–74.
4 Tsukada S, Parsons CJ, Rippe RA. Mechanisms of liver fibrosis. *Clin Chim Acta* 2006; **364**: 33–60.
5 Inagaki Y, Higashiyama R, Higashi K. Novel anti-fibrotic modalities for liver fibrosis: molecular targeting and regenerative medicine in fibrosis therapy. *J Gastroenterol Hepatol* 2012; **27** (Suppl 2): 85–8.
6 Bonner JC. Regulation of PDGF and its receptors in fibrotic diseases. *Cytokine Growth Factor Rev* 2004; **15**: 255–73.
7 Tsukamoto H. Cytokine regulation of hepatic stellate cells in liver fibrosis. *Alcohol Clin Exp Res* 1999; **23**: 911–6.
8 Novobrantseva TI, Majeau GR, Amatucci A *et al.* Attenuated liver fibrosis in the absence of B cells. *J Clin Invest* 2005; **115**: 3072–82.
9 Bataller R, Brenner DA. Hepatic stellate cells as a target for the treatment of liver fibrosis. *Semin Liver Dis* 2001; **21**: 437–51.
10 Friedman SL. Liver fibrosis – from bench to bedside. *J Hepatol* 2003; **38** (Suppl 1): S38–53.
11 Zhang D, Utsumi T, Huang HC *et al.* Reticulon 4B (Nogo-B) is a novel regulator of hepatic fibrosis. *Hepatology* 2011; **53**: 1306–15.
12 Kambayashi J, Liu YG, Sun B, Shakur Y, Yoshitake M, Czerwiec F. Cilostazol as a unique antithrombotic agent. *Curr Pharm Des* 2003; **9**: 2289–302.
13 Okuda Y, Mizutani M, Ikegami T, Ueno E, Yamashita K. Hemodynamic effects of cilostazol on peripheral artery in patients with diabetic neuropathy. *Arzneimittelforschung* 1992; **42**: 540–2.
14 Wang S, Cone J, Fong M, Yoshitake M, Kambayashi J, Liu YG. Interplay between inhibition of adenosine uptake and phosphodiesterase type 3 on cardiac function by cilostazol, an agent to treat intermittent claudication. *J Cardiovasc Pharmacol* 2001; **38**: 775–83.
15 Kimura Y, Tani T, Kanbe T, Watanabe K. Effect of cilostazol on platelet aggregation and experimental thrombosis. *Arzneimittelforschung* 1985; **35**: 1144–9.
16 Kohriyama T, Tanaka E, Katayama S, Yamamura Y, Nakamura S. [Antiplatelet therapy in patients with cerebral thrombosis at the chronic phase – assessment of its effect on coagulation and fibrinolytic parameters]. *Rinsho Shinkeigaku* 1994; **34**: 771–6.

17 Liu Y, Cone J, Le SN *et al.* Cilostazol and dipyridamole synergistically inhibit human platelet aggregation. *J Cardiovasc Pharmacol* 2004; **44:** 266–73.
18 Liu Y, Shakur Y, Yoshitake M, Kambayashi Ji J. Cilostazol (pletal): a dual inhibitor of cyclic nucleotide phosphodiesterase type 3 and adenosine uptake. *Cardiovasc Drug Rev* 2001; **19:** 369–86.
19 Mizutani M, Okuda Y, Yamashita K. Effect of cilostazol on the production of platelet-derived growth factor in cultured human vascular endothelial cells. *Biochem Mol Med* 1996; **57:** 156–8.
20 Bender AT, Beavo JA. Cyclic nucleotide phosphodiesterases: molecular regulation to clinical use. *Pharmacol Rev* 2006; **58:** 488–520.
21 Hayashi S, Morishita R, Matsushita H *et al.* Cyclic AMP inhibited proliferation of human aortic vascular smooth muscle cells, accompanied by induction of p53 and p21. *Hypertension* 2000; **35:** 237–43.
22 Kawada N, Kuroki T, Kobayashi K, Inoue M, Kaneda K. Inhibition of myofibroblastic transformation of cultured rat hepatic stellate cells by methylxanthines and dibutyryl cAMP. *Dig Dis Sci* 1996; **41:** 1022–9.
23 Mallat A, Preaux AM, Serradeil-Le Gal C *et al.* Growth inhibitory properties of endothelin-1 in activated human hepatic stellate cells: a cyclic adenosine monophosphate-mediated pathway. Inhibition of both extracellular signal-regulated kinase and c-Jun kinase and upregulation of endothelin B receptors. *J Clin Invest* 1996; **98:** 2771–8.
24 Houglum K, Lee KS, Chojkier M. Proliferation of hepatic stellate cells is inhibited by phosphorylation of CREB on serine 133. *J Clin Invest* 1997; **99:** 1322–8.
25 Shimizu E, Kobayashi Y, Oki Y, Kawasaki T, Yoshimi T, Nakamura H. OPC-13013, a cyclic nucleotide phosphodiesterase type III, inhibitor, inhibits cell proliferation and transdifferentiation of cultured rat hepatic stellate cells. *Life Sci* 1999; **64:** 2081–8.
26 Fujita K, Nozaki Y, Wada K *et al.* Effectiveness of antiplatelet drugs against experimental non-alcoholic fatty liver disease. *Gut* 2008; **57:** 1583–91.
27 Hase Y, Okamoto Y, Fujita Y *et al.* Cilostazol, a phosphodiesterase inhibitor, prevents no-reflow and hemorrhage in mice with focal cerebral ischemia. *Exp Neurol* 2012; **233:** 523–33.
28 Hasegawa SI, Inomata J, Tuji Y, Saitoh E. Assessment of buccal absorption of cilostazol 100-mg orally disintegrated tablets in healthy adult male subjects. *Jpn Pharmacol Ther* 2009; **37:** 813–9.
29 Hasegawa SI, Inomata J, Tuji Y, Saitoh E. Bioequivalence study of cilostazol 100-mg orally disintegrated tablets and cilostazol 100-mg conventional tablets in healthy adult male subjects. *Jpn Pharmacol Ther* 2009; **37:** 805–12.
30 Isayama F, Hines IN, Kremer M *et al.* LPS signaling enhances hepatic fibrogenesis caused by experimental cholestasis in mice. *Am J Physiol Gastrointest Liver Physiol* 2006; **290:** G1318–28.
31 Toda Y, Kono K, Abiru H *et al.* Application of tyramide signal amplification system to immunohistochemistry: a potent method to localize antigens that are not detectable by ordinary method. *Pathol Int* 1999; **49:** 479–83.
32 Seki E, De Minicis S, Osterreicher CH *et al.* TLR4 enhances TGF-beta signaling and hepatic fibrosis. *Nat Med* 2007; **13:** 1324–32.
33 Schnabl B, Kweon YO, Frederick JP, Wang XF, Rippe RA, Brenner DA. The role of Smad3 in mediating mouse hepatic stellate cell activation. *Hepatology* 2001; **34:** 89–100.
34 Siegmund SV, Uchinami H, Osawa Y, Brenner DA, Schwabe RF. Anandamide induces necrosis in primary hepatic stellate cells. *Hepatology* 2005; **41:** 1085–95.
35 Weiskirchen R, Gressner AM. Isolation and culture of hepatic stellate cells. *Methods Mol Med* 2005; **117:** 99–113.
36 Friedman SL, Roll FJ. Isolation and culture of hepatic lipocytes, Kupffer cells, and sinusoidal endothelial cells by density gradient centrifugation with Stractan. *Anal Biochem* 1987; **161:** 207–18.
37 Mou L, Xing Y, Kong Z, Zhou Y, Chen Z, Wang R. The N-terminal domain of human hemokinin-1 influences functional selectivity property for tachykinin receptor neurokinin-1. *Biochem Pharmacol* 2011; **81:** 661–8.
38 Tomita K, Tamiya G, Ando S *et al.* Tumour necrosis factor alpha signalling through activation of Kupffer cells plays an essential role in liver fibrosis of non-alcoholic steatohepatitis in mice. *Gut* 2006; **55:** 415–24.
39 Friedman SL, Arthur MJ. Activation of cultured rat hepatic lipocytes by Kupffer cell conditioned medium. Direct enhancement of matrix synthesis and stimulation of cell proliferation via induction of platelet-derived growth factor receptors. *J Clin Invest* 1989; **84:** 1780–5.
40 Tsukamoto H, Gaal K, French SW. Insights into the pathogenesis of alcoholic liver necrosis and fibrosis: status report. *Hepatology* 1990; **12:** 599–608.
41 Wong L, Yamasaki G, Johnson RJ, Friedman SL. Induction of beta-platelet-derived growth factor receptor in rat hepatic lipocytes during cellular activation in vivo and in culture. *J Clin Invest* 1994; **94:** 1563–9.
42 Borkham-Kamphorst E, van Roeyen CR, Ostendorf T, Floege J, Gressner AM, Weiskirchen R. Pro-fibrogenic potential of PDGF-D in liver fibrosis. *J Hepatol* 2007; **46:** 1064–74.
43 Melton AC, Yee HF. Hepatic stellate cell protrusions couple platelet-derived growth factor-BB to chemotaxis. *Hepatology* 2007; **45:** 1446–53.
44 Yasuda Y, Shimizu M, Sakai H *et al.* (-)-Epigallocatechin gallate prevents carbon tetrachloride-induced rat hepatic fibrosis by inhibiting the expression of the PDGFRbeta and IGF-1R. *Chem Biol Interact* 2009; **182:** 159–64.
45 Gonzalo T, Beljaars L, van de Bovenkamp M *et al.* Local inhibition of liver fibrosis by specific delivery of a platelet-derived growth factor kinase inhibitor to hepatic stellate cells. *J Pharmacol Exp Ther* 2007; **321:** 856–65.

46 Yoshiji H, Noguchi R, Kuriyama S *et al.* Imatinib mesylate (STI-571) attenuates liver fibrosis development in rats. *Am J Physiol Gastrointest Liver Physiol* 2005; **288**: G907–13.
47 Graves LM, Bornfeldt KE, Raines EW *et al.* Protein kinase A antagonizes platelet-derived growth factor-induced signaling by mitogen-activated protein kinase in human arterial smooth muscle cells. *Proc Natl Acad Sci U S A* 1993; **90**: 10300–4.
48 Mallat A, Gallois C, Tao J *et al.* Platelet-derived growth factor-BB and thrombin generate positive and negative signals for human hepatic stellate cell proliferation. Role of a prostaglandin/cyclic AMP pathway and cross-talk with endothelin receptors. *J Biol Chem* 1998; **273**: 27300–5.

SUPPORTING INFORMATION

ADDITIONAL SUPPORTING INFORMATION may be found in the online version of this article at the publisher's web-site:

Video Clip S1–S3 Time-lapse motion pictures of cultured hepatic stellate cells (HSC) with or without cilostazol treatment.

Nutrition 30 (2014) 1195–1207

Contents lists available at ScienceDirect

Nutrition

journal homepage: www.nutritionjrnl.com

Basic nutritional investigation

Whey-hydrolyzed peptide-enriched immunomodulating diet prevents progression of liver cirrhosis in rats

Kanta Jobara M.D.[a], Toshimi Kaido M.D., Ph.D.[a,*], Tomohide Hori M.D., Ph.D.[a], Keiko Iwaisako M.D., Ph.D.[b], Kosuke Endo M.D.[a], Yoichiro Uchida M.D., Ph.D.[a], Shinji Uemoto M.D., Ph.D.[a]

[a] *Division of Hepato-Biliary-Pancreatic and Transplant Surgery, Department of Surgery, Kyoto University Graduate School of Medicine, Kyoto, Japan*

[b] *Department of Target Therapy Oncology, Kyoto University Graduate School of Medicine, Kyoto, Japan*

ARTICLE INFO

Article history:
Received 14 September 2013
Accepted 5 February 2014

Keywords:
Whey-hydrolyzed peptide
Immunomodulating diet
Liver fibrosis
Cirrhosis
Antifibrotic
Hepatocytes-protective

ABSTRACT

Objective: Liver fibrosis and subsequent cirrhosis is a major cause of death worldwide, but few effective antifibrotic therapies are reported. Whey-hydrolyzed peptide (WHP), a major peptide component of bovine milk, exerts anti-inflammatory effects in experimental models. A WHP-enriched diet is widely used for immunomodulating diets (IMD) in clinical fields. However, the effects of WHP on liver fibrosis remain unknown. The aim of this study was to investigate the antifibrotic effects of WHP in a rat cirrhosis model.

Methods: Progressive liver fibrosis was induced by repeated intraperitoneal administration of dimethylnitrosamine (DMN) for 3 wk. Rats were fed either a WHP-enriched IMD (WHP group) or a control enteral diet (control group). The degree of liver fibrosis was compared between groups. Hepatocyte-protective effects were examined using hepatocytes isolated from rats fed a WHP diet. Reactive oxygen species and glutathione in liver tissue were investigated in the DMN cirrhosis model.

Results: Macroscopic and microscopic progression of liver fibrosis was remarkably suppressed in the WHP group. Elevated serum levels of liver enzymes and hyaluronic acid, and liver tissue hydroxyproline content were significantly attenuated in the WHP group. Necrotic hepatocyte rates with DMN challenge, isolated from rats fed a WHP-enriched IMD, were significantly lower. In the DMN cirrhosis model, reactive oxygen species were significantly lower, and glutathione was significantly higher in the WHP group's whole liver tissue.

Conclusion: A WHP-enriched IMD effectively prevented progression of DMN-induced liver fibrosis in rats via a direct hepatocyte-protective effect and an antioxidant effect through glutathione synthesis.

Introduction

Liver cirrhosis is the end stage of chronic liver injury resulting from various causes, such as viral or alcoholic hepatitis, and non-alcoholic steatohepatitis [1]. It is histopathologically characterized as the loss of hepatocytes with interstitial fibrosis [2]. Progression of fibrosis and subsequent cirrhosis lead to life-threatening liver failure and carcinogenesis [1,3]. Despite extensive research on liver cirrhosis, there are few medications (without adverse side effects) proven to be clinically useful for prevention or slowing the progression of liver fibrosis [4,5]. Therefore, new antifibrotic agents with less toxicity are needed for the management and prevention of liver fibrosis [6].

Continuous hepatocellular damage caused by virus and alcohol introduces an inflammatory response with release of inflammatory cytokines, such as interleukin (IL)-6, tumor necrosis factor (TNF)-α, and IL-10. These inflammatory cytokines promote remodeling and macrophage phagocytosis of necrotic hepatocytes. Subsequent activation of hepatic stellate cells (HSCs) by transforming growth factor (TGF)-β promotes

KJ, TK, and KI designed the research. TK, TH, and SU conducted the research. KJ, TK, TH, KI, KE, and YU analyzed the data. KJ wrote the initial draft. KJ, TK, TH, and KI reworked further drafts, and TK and SU had primary responsibility for the final content. All authors read and approved the final manuscript.

* Corresponding author. Tel.: +81 75 751 4322; fax: +81 75 751 4348.
E-mail address: Kaido@kuhp.kyoto-u.ac.jp (T. Kaido).

0899-9007/$ - see front matter © 2014 Elsevier Inc. All rights reserved.
http://dx.doi.org/10.1016/j.nut.2014.02.005

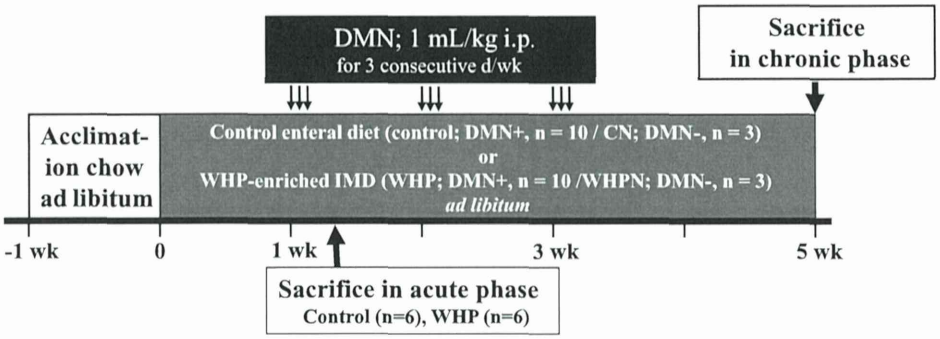

Fig. 1. Experimental protocols in vivo. CN, control diet without DMN as negative control for DMN; DMN, dimethylnitrosamine; IMD, immunomodulating diet; WHP, whey-hydrolyzed peptide; WHPN, whey-hydrolyzed peptide diet without DMN as negative control for DMN.

production extracellular matrix and leads to liver fibrosis [7,8]. Reactive oxygen species (ROS) are involved in liver injury, and antioxidants may protect hepatocytes and prevent following liver fibrosis [9]. Moreover, hepatocellular damages and inflammatory cytokines interact with each other.

Recent nutritional studies demonstrated that bovine milk proteins have many effects for health benefits, such as preventing weight gain and enhancing bone architecture [10]. Whey-hydrolyzed peptide (WHP) is a major peptide component of bovine milk. A WHP-enriched diet is one form of immunomodulating diet (IMD) that has been widely used for nutritional support in patients with malnutrition or insufficient oral intake. A WHP-enriched IMD exerts antioxidant, anti-inflammatory, immunomodulating, and antibacterial effects in some experimental models [11–15]. The clinical utility of this novel WHP-enriched IMD has been documented, mainly at the perioperative period [16–18]. Previous research has indicated that a WHP-enriched diet exerts an anti-inflammatory effect, and may have therapeutic potential [11].

The present study investigated the antifibrotic effects of WHP in a rat liver cirrhosis model with progressive fibrosis. We also discuss the therapeutic potential of WHP against progressive fibrosis and possible mechanisms during liver cirrhosis progression from a literature review.

Materials and methods

Rats

Male Sprague-Dawley rats (6 wk old) were purchased from Japan SLC, Inc. (Hamamatsu, Japan). Rats were cared for according to the Institutional Guidelines for Animal Welfare. All experimental procedures were approved by the Institutional Animal Care and Use Committee of Kyoto University (Protocol ID: MedKyo12521).

Immunomodulating diet

Rats were fed conventional chow as a control enteral diet (MEIBALANCE; Meiji Dairies Co., Tokyo, Japan) or a WHP-enriched IMD (MEIN; Meiji Dairies Co.) ad libitum throughout the experiments (Fig. 1). The compositions of the two diets were almost identical, except for the protein source as summarized in Table 1 (casein in the control diet, and WHP in the WHP-enriched IMD).

Liver cirrhosis model rats

One week after starting diets, rats were intraperitoneally given dimethylnitrosamine (DMN; 1% dissolved in saline; 1 mL/kg; Tokyo Chemical Industry Co. Ltd., Tokyo, Japan) consecutively for 3 d each week for 3 wk to induce progressive fibrosis and subsequent cirrhosis [19,20] (Fig. 1).

Histopathologic assessment

Liver specimens were fixed in 4% paraformaldehyde, embedded in paraffin, serially cut into thin slices (3 μm thick). Slides were stained with hematoxylin

Table 1
Diet composition*

	Control	WHP-enriched IMD
Proteins (g)	5.0	5.0
Protein (% kcal)	20.0	20.0
Protein sources	Total milk protein Na caseinate	Whey peptides Fermented milk
Carbohydrates (g)	15.3	14.5
Carbohydrates (% kcal)	57.5	55
CHO sources	Dextrin	Isomaltulose Dextrin
Lipids (g)	2.50	2.80
Lipids (% kcal)	22.5	25.0
MCT (g)	-	0.59
EPA, DHA (g)	-	0.060
ω-6/ω-3	3.2	2.0
Vitamins		
Vitamin A (g RE)	60.0	150
Vitamin D (g)	0.50	0.75
Vitamin E (mg)	3.0	5.0
Vitamin K (g)	5.0	3.4
Vitamin B1 (mg)	0.15	0.25
Vitamin B2 (mg)	0.20	0.30
Niacin (mg)	1.6	3.0
Vitamin B6 (mg)	0.30	0.30
Vitamin B12 (g)	0.60	0.60
Folic acid (g)	50	50
Biotin (g)	15	7.5
Pantothenic acid	0.60	1.2
Vitamin C (mg)	16	50
Choline (mg)	1.8	9.2
Carnitine (mg)	-	15
Minerals		
Sodium (mg)	110	70
Potassium (mg)	100	80
Calcium (mg)	70	80
Magnesium (mg)	30	20
Phosphorus (mg)	70	70
Iron (mg)	1.0	1.0
Zinc (mg)	1.0	1.0
Copper (mg)	0.050	0.050
Manganese (mg)	0.230	0.175
Chromium (g)	3.00	2.96
Molybdenum (g)	2.5	2.5
Selenium (g)	6.0	5.0
Iodine (g)	15	9.7
Chloride (mg)	110	80

CHO, carbohydrate; DHA, docosahexaenoic acid; EPA, eicosapentaenoic acid; IMD, immunomodulating diet; RE, retinol equivalent; MCT, medium chain triglyceride; WHP, whey-hydrolyzed peptide; (-), no additives

* The major difference between WHP-enriched IMD and control enteral diet used in this study is the protein composition; the WHP-enriched IMD contains whey peptides and fermented milk product as the protein sources, whereas the control enteral diet contains total milk protein and sodium caseinate.

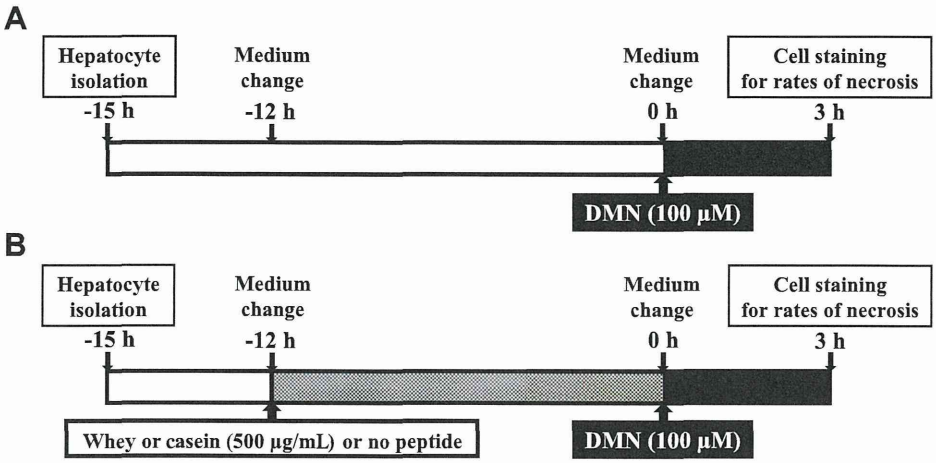

Fig. 2. Protocol for analysis of the hepatocyte-protective effect. (A) Protocol for analysis of the hepatocyte-protective effect in vivo for isolated hepatocytes from rats fed a WHP diet. (B) Protocol for analysis of the hepatocyte-protective effect in vitro for hepatocytes with WHP-added medium. DMN, dimethylnitrosamine; WHP, whey-hydrolyzed peptide.

and eosin and Mallory–Azan stain for histologic analysis of fibrosis. The degrees of liver fibrosis and histologic activity in native livers were scored according to the Metavir scoring system [21].

Immunohistochemistry

After blocking, sections were incubated with a primary antibody for α-smooth muscle actin (α-SMA) (ab5694; Abcam, Cambridge, UK) and then with a labeled polymer (Envision System/Horse radish peroxidase; Dako, Tokyo, Japan). Sections were examined after incubation with diamino benzidine (Liquid Diamino Benzidine Substrate Chromogen System; Dako). The α-SMA staining was analyzed using quantitative software (BZ-Analyzer; KEYENCE, Osaka, Japan), with detection thresholds set to the brown color (diamino benzidine color). Images of five non-overlapping fields were selected at random and captured per section at ×200 magnification. The degree of labeling in each section was determined from the area within the color range divided by the total area. For collagen I, we used primary antibody against collagen I (NB600-408; Novus Biologicals, Littleton, CO, USA) with biotinylated antibody-recognizing rabbit immunoglobulin G (BA-1000; Vector Laboratories, Burlingame, CA, USA). The positive areas of the staining were analyzed by quantitative software in the same way as α-SMA staining.

Hydroxyproline determination

For collagen quantification in the liver, hydroxyproline (the specific amino acid of type I collagen) was measured using the standard biochemical method described previously [22] Hydroxyproline was then quantitated photometrically at 558 nm from a standard curve generated using purified hydroxyproline (Sigma, Tokyo, Japan).

Hepatocyte isolation

Hepatocytes were isolated from rat livers as previously described [23,24]. Briefly, rat liver was perfused for 15 min with 0.03% collagenase (Wako, Kyoto, Japan). After collagenase perfusion, the cell suspension was centrifuged at 50*g* for 1 min.

Cell culture

Isolated hepatocytes were cultured on six-well plates coated with type I collagen at a cell density of 1×10^5 cells/well with serum-free Medium 199 Earle's liquid (Invitrogen, Tokyo, Japan), 100 U/mL penicillin, 100 μg/mL streptomycin, and 0.25 μg/mL of amphotericin B at 37°C.

Propidium iodide Hoechst ratio calculation for degree of hepatocyte necrosis

Cultured hepatocytes were stained with Hoechst 33342 (Nacalai Tesque, Kyoto, Japan) and propidium iodide (Calbiochem, San Diego, CA, USA) for DNA staining to evaluate cell viability. Double staining with propidium iodide (for dead cells) and Hoechst 33342 (for dead and viable cells) was used to differentiate necrotic cells from normal cells with a fluorescent microscope. Images of five non-overlapping fields at ×200 magnification were selected at random, and cells were automatically counted (BZ-II Analyzer; KEYENCE). The propidium iodide-positive ratio was calculated as the percentage of propidium iodide-positive cells among Hoechst 33342-positive cells [24].

Inflammatory cytokines in serum

Serum concentrations of IL-6, TNF-α, IL-10, and interferon (IFN)-γ were measured using conventional assay kits (Cytometric Bead Array Kits; Becton Dickinson Co., Franklin Lakes, NJ, USA).

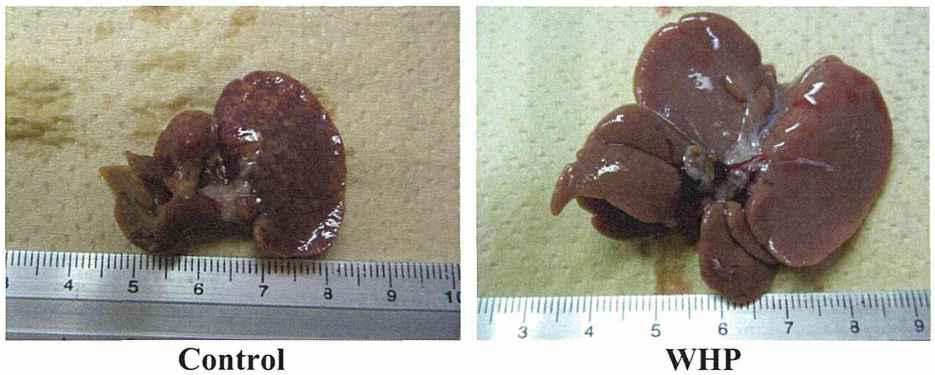

Fig. 3. Antifibrotic/cirrhotic effects of WHP in macroscopic findings of livers in the DMN-induced cirrhosis rat model (chronic phase). In the control group, a granular liver surface and remarkable atrophy were observed. Livers from the WHP group showed near normal findings and a non-damaged appearance. DMN, dimethylnitrosamine; WHP, whey-hydrolyzed peptide.